buildings

MDPI

Article

Optimal Quantity Investigation of Metakaolin and Silica Fume in Production of Durable Acid Resistance Alkali Activated Slag Concrete

Abolfazl Azmakan [1], Jamal Ahmadi [1], Arash Shahani [1], Baitollah Badarloo [2] and Tomasz Garbowski [3,*]

[1] Department of Structural Engineering, Faculty of Civil and Survey Engineering, University of Zanjan, Zanjan 45371-38791, Iran; a.azmakan@znu.ac.ir (A.A.); j_ahmadi@znu.ac.ir (J.A.); arash.shahani@znu.ac.ir (A.S.)
[2] Department of Civil Engineering, Qom University of Technology (QUT), Qom 37181-46645, Iran; badarloo@qut.ac.ir
[3] Department of Biosystems Engineering, Poznan University of Life Sciences, Wojska Polskiego 50, 60-627 Poznan, Poland
* Correspondence: tomasz.garbowski@up.poznan.pl

Abstract: The urgent requirement to reduce greenhouse gas emissions during Portland cement production and to enhance the durability of concrete in destructive environments are essential reasons to seek other alternative materials like alkaline activated binders. In this study, the feasibility of producing durable alkali-activated slag-based concrete under deteriorative environmental conditions was studied using 0, 10, 20, 30, and 40% of metakaolin (MK) and 0, 5, and 10% of silica fume (SF) instead of ground granulated blast furnace slag (GGBFS) and optimizing contents through the response surface method (RSM).To evaluate the performance of studied alkali-activated slag-based concrete in an aggressive environment, the permeability and the reduction in compressive strength of alkali-activated slag-based concrete under sulfuric acid attack have been investigated. In addition, the mass change of specimens after exposure was measured. The results indicate that replacing 40% of the slag with metakaolin and 10% with silica fume in alkali-activated concrete has reduced 9% and 34.9% of the compressive strength at 28 days, respectively. Also, increasing MK replacement up to 40% increased the water absorption to 27.8%, but 10% SF replacement reduced it to 17.7%. In addition, the alkali-activated slag-based concrete mass changes after 90 days of acid exposure were 2.3%, while the replacement of slag by 40% of MK and 10% of SF reduced this value to 1.14%. However, it improved the durability performance of alkali-activated concrete against sulfuric acid attacks.

Keywords: alkali activated concrete; metakaolin; durability; acid attack; optimization

Citation: Azmakan, A.; Ahmadi, J.; Shahani, A.; Badarloo, B.; Garbowski, T. Optimal Quantity Investigation of Metakaolin and Silica Fume in Production of Durable Acid Resistance Alkali Activated Slag Concrete. *Buildings* **2024**, *14*, 21. https://doi.org/10.3390/buildings14010021

Academic Editor: Denny Coffetti

Received: 30 October 2023
Revised: 10 December 2023
Accepted: 15 December 2023
Published: 20 December 2023

1. Introduction

Despite its unique features, the development of Portland cement concrete as the 21st-century primary building material faces certain restrictions. As the most widely used binder in concrete for construction applications, Portland cement production is a very energy-consuming process that is estimated to be responsible for significant amounts of greenhouse gas emissions [1–3]. In addition, the performance of Portland cement concrete when exposed to corrosive and invasive environments, such as acid attacks, is worrying [4]. However, not only is this building material still considered the foremost opportunity to meet the growing needs of human societies, but it is also considered a product for the consumption of by-products such as silica fume, fly ash, smelting furnace slag, glass, and rubber in other industrial sectors [5]. Considering the mentioned restrictions and demands, the necessity to use alternative cement materials with environmental compatibility and elevated/enhanced features seems essential [6,7].

In 1979, Davidovits proposed the concept of geopolymers that can be produced by reacting alumina and silicate materials with alkaline-activating solutions [8,9]. Alkali-activated and geopolymer concretes, as a recent valuable human achievement in producing environmentally friendly concrete, have the potential to be replaced entirely with Portland cement [10]. Estimates reveal that carbon dioxide emitted into the air from Portland cement production can be decreased by up to 80% by employing modern cement technologies such as geopolymers and alkali-activated binders [11].

Alkali-activated slag (AAS) binders and Portland cement (PC) are two primary types of hydraulic binders used in construction materials, particularly concrete [12]. Despite serving a similar purpose, these binders exhibit distinct chemical compositions, reaction mechanisms, and properties that influence their performance in various applications. AAS binders are produced by activating ground granulated blast furnace slag (GGBFS) with an alkaline activator, typically sodium hydroxide (NaOH) or sodium silicate (Na_2SiO_3) [13]. The typical chemical composition of AAS binders includes GGBS, an alkaline activator, and water [14]. PC, on the other hand, is manufactured by heating a mixture of limestone ($CaCO_3$), clay (Al_2SiO_4), and iron oxide (Fe_2O_3) to 1450 °C [15]. The resulting clinker is then ground with additives to produce PC [16]. The typical chemical composition of PC includes tricalcium silicate (C_3S), dicalcium silicate (C_2S), tricalcium aluminate (C_3A), calcium aluminoferrite (C_4AF), and other minor phases [15,16].

Alkali-activated binders are produced by mixing solid alumino-silicate powders such as fly ash, metakaolin, and blast furnace slag (BFS) with an active alkaline solution. This adhesive's mechanical properties and microstructural composition depend on the raw materials' chemical composition, the amount of alkaline activator, and its concentration [17]. This concrete can be divided into two main categories. The first class consists of high calcium systems, like blast furnace slag with mild alkaline solutions, which is the main product of this C-S-H gel reaction [18]. The second category is low-calcium or calcium-free systems with medium to high alkalinity solutions, which are the most suitable materials among the sources of alumino-silicate, metakaolin, and F-type fly ash. This group produces a polymeric structure (N-A-S-H) similar to zeolite [8]. Studies have shown significant improvement in compressive strength and lower micro-cracks by adding an alumino-silicate source into an alkali-activated slag concrete system [19–21].

The previously mentioned materials are used to reduce cement consumption and prevent environmental pollution induced by the construction industry [22]. Despite being produced without Portland cement, geopolymer concrete has displayed equal or even improved strength than ordinary Portland cement concrete [11,23–26]. However, Xu and Van Deventer [27] point out that in most cases, the dissolution rate of Al in natural alumino-silicate is insufficient to produce a suitable composite gel. In this regard, Lee et al. [28] evaluated the mechanical properties of ash-based geopolymer concrete and its replacement with different slag content. Their results revealed that increasing the slag containing large amounts of CaO improved the setting time and compressive strength. They described the reason as the presence of CaO and the formation of a gel with an amorphous Ca-Al-Si structure, which increases the compressive strength of polymer concrete. Bernal et al. [29] replaced 0, 10, and 20% of the slag paste activated by sodium silicate and sodium hydroxide with metakaolin. They reported that using metakaolin in the AAS-activated alkaline slag matrix reduces compressive strength and speeds up hydration. Wang et al. [30] investigated the compressive strength and porosity of alkali-activated slag concrete, metakaolin, and fly ash activated with sodium silicate and sodium hydroxide. The sodium silicate to sodium hydroxide and water-to-solids ratios were considered 1 and 0.35, respectively. In different specimens, they used the various contents of slag, fly ash, and metakaolin. They reported that increasing the slag content increased the specimens' density and compressive strength, as higher amounts of slag in the system increased hydrated products (C-S-H and hydrated calcium aluminate). On the other hand, the ratio of alkaline solution to the binder, molarity, NaOH content, ratio of sodium silicate to sodium hydroxide, curing temperature, and concrete age substantially affect the compressive strength of geopolymer concrete [31,32].

Yip et al. [19] studied the effects of adding smelting furnace slag to a metakaolin-based geopolymer concrete. Using scanning electron microscopy, they investigated different amounts of slag impact on the concrete's microstructure and strength. They observed that the geopolymer surface has more microcracks and pores than the surface with calcium (C-S-H). Chao et al. [33] reported that due to the very high surface area and plate-like shape of metakaolin particles, water demand is very high in concrete with metakaolin content, which causes drying shrinkage problems.

Evaluating the durability of geopolymer and alkali concretes active in hazardous environments has been another topic of interest for researchers in this field. In this regard, Timothy et al. examined the effect of replacement and increased slag content and alkali-activating dose on the compressive strength of low-calcium fly ash-based geopolymer specimens against sulfuric acid compared to OPC concrete [34]. Their results showed that increasing the slag replacement with fly ash reduces porosity and increases the vulnerability of reaction products to sulfuric acid. Also, with increasing the dose of the alkali-activator, the positive effect of fly ash against sulfuric acid solution has decreased. They reported that the OPC specimens experienced the most significant damage against sulfuric acid. As calcium hydroxide and C-S-H with a high Ca/Si ratio are prone to maximum damage against the sulfuric acid solution, they concluded that the nature of hydration products significantly reduces the compressive strength of the specimens against sulfuric acid [35]. Consequently, the most noticeable advantage of geopolymer materials such as metakaolin and fly ash against sulfuric acid is their low calcium oxide than OPC and slag materials.

Several input factors are at different levels in active alkali concrete, significantly impacting the hardened concrete properties. Predominantly, the trial and error method is a commonly used approach to identify influential input factors in the concrete mix proportions/design. However, the trial and error method requires considerable experiment efforts, leading to increased time, cost, and material consumption [36]. Accordingly, employing creative approaches to provide optimal experimental design is essential to attain particular objectives [37]. To tackle this problem, different techniques, such as the response level optimization approach, have been employed recently. Response level optimization is a combination of mathematical and statistical techniques. This technique is appropriate for modeling and analyzing problems in which the response variable is affected by multiple inputs, aiming to optimize the response [38,39].

Although alkali-activated slag-based (AAS) concretes offer environmental benefits, their durability, permeability, and manufacturing consistency must be improved for broader use in aggressive environments, such as sulfuric acids. One of the main factors that deteriorate concrete in sulfuric acid is the reactivity of calcium ions released from hardened cement gel with sulfates present in the acidic environment, producing expansive products such as gypsum. Reducing the amount of calcium oxide in alkali-activated concrete precursors, provided that the conditions required for producing hardened products are not compromised, can improve the durability of concrete against acid attack. Therefore, selecting the precursor replacing slag for alkaline activation and determining its optimum values is particularly important.

This study uses statistical analysis response surface m ethodology (RSM) to evaluate the mechanical properties of alkali-activated slag concrete specimens against the sulfuric acid solution. Metakaolin, as a source of alumino-silicate, and silica fume were used as the replacement for part of the slag in the alkali-activated slag concrete. Also, their effect on compressive strength against sulfuric acid has been investigated. The parameters such as compressive strength, water absorption (including initial and final volumetric and capillary water absorption), and mass reduction of the sulfuric acid-immersed specimens were tested to evaluate the mechanical performance. Furthermore, the decrease in compressive strength has also been calculated to evaluate the durability of concrete in the cited environment. Furthermore, scanning electron microscopy (SEM) analysis was performed on the specimens to evaluate their microstructures.

2. Materials, Methods, and Experimental Program

In addition to laboratory tests, the physical and chemical features of the materials utilized to produce alkali-activated concrete have been discussed in this section. Moreover, the ratio of alkaline activator solutions and the studied mix designs have been explained in detail.

2.1. Materials

In this study, ground granulated blast furnace slag (Slag: The slag was from the blast furnace of "Isfahan Iron and Steel Company", which was milled in "Kurdistan Cement Factory") (GGBFS), with a specific weight of 2850 kg/m^3 and with a blain of 4500 cm^2/g, was used for specimens' preparation of alkaline-activated concrete (Table 1). The silica fume (Silica fume: Silica fume powder was from "Azna Silica Fume") used is light gray and granular, with a particle size of less than 1 µm and a specific surface area of 15–30 m^2/g. This material is amorphous, with a bulk density ranging from 310 to 350 kg/m^3, a specific density of 2.2, and pozzolanic activity of 80 to 105%. The metakaolin (Metakaolin: In this study, metakaolin was from the "Technical and Specialized Concrete Company of Iran") is also non-densified granular, with a specific surface area of 12–13 m^2/g and approximately 85% pozzolanic activity. This material has been thermally activated at about 700 to 800 °C. A combination of sodium silicate (Sodium silicate: This study used liquid sodium silicate from "Iran Silicon Industries Company", with Ratio = 2.4) (Na_2SiO_3) with SiO_2/Na_2O = 2.4 (SiO_2 = 36.7%, Na_2O = 15.3%, H_2O = 48%, and sodium hydroxide (Sodium hydroxide: In this study, solid flake soda from "Tabesh Chemistry Dynamic Company" with a purity of 98% was used) (NaOH) with a purity of 98% and a molar concentration of 14 M (Na^{2+} = 24.64%, OH^- = 18.22% and H_2O = 56.25%) were used to activate slag. The sodium silicate to sodium hydroxide ratio was 2. Natural crushed stone with a maximum diameter of 19 mm, density of 2760 kg/m^3, and water absorption of 1.8% was used as coarse aggregate in concrete production, according to ASTM C127 [40]. The fine aggregates were river sand with density and fineness modulus of 2520 kg/m^3 and 3.62, respectively, according to ASTM C33 [41]. Moreover, a naphthalene-based superplasticizer was added to the mixed designs to maintain a 100–120 mm slump. Furthermore, with the specifications displayed in Table 1, silica fume and metakaolin have been used as a source of alumino-silicate.

Table 1. Chemical compositions of GGBFS, metakaolin, and silica fume (%).

Material	SiO_2	Al_2O_3	CaO	Fe_2O_3	MgO	SO_3	MnO	Etc.
GGBFS	35.43	9.17	38.23	0.81	8.67	2.5	1.34	3.85
Metakaolin	48.00	41.00	3.10	1.30	1.80	0.20	-	4.6
Silica fume	96.4	1.32	0.49	0.87	0.97	0.10	-	-

2.2. Methods

In this study, specimens consisting of 1680 kg/m^3 of coarse and fine aggregates with equal amounts of 840 kg/m^3 were used to prepare specimens of alkali-activated concrete based on slag and investigate the effect of aluminosilicate content. The ratio of alkaline solution to cementitious and pozzolanic materials was considered to be 0.4, which was equal to 163.5 kg/m^3. Also, 148 kg/m^3 of additional water was used to provide a ratio of 0.48 water to the total solid materials of the binder (including sodium silicate solutions, sodium hydroxide solutions, latent cementitious and pozzolanic materials). Also, to investigate the effects of silica fume and metakaolin, the slag in the concrete mixture was replaced with different amounts of these minerals. The experimental results were obtained from the capillary water absorption test, performed according to RILEM TC 116-PCD [42]. The key parameters for measuring capillary absorption were the weight of the oven-dried specimen, the capillary water-absorbed specimen, and the time intervals.

Compressive strength values were determined from 10 × 10 × 10 cm cubic samples according to BS 1881-116 [43] at 7, 28, 60, 90, and 120 days. Initial water absorption according to BS 1881-122 [44], and final water absorption according to ASTM C642 [45] were calculated at 7 and 28 days, respectively. Mass changes of the specimens were also measured to investigate the effect of acid attack on concrete specimens. Several parts of this research are shown in Figure 1.

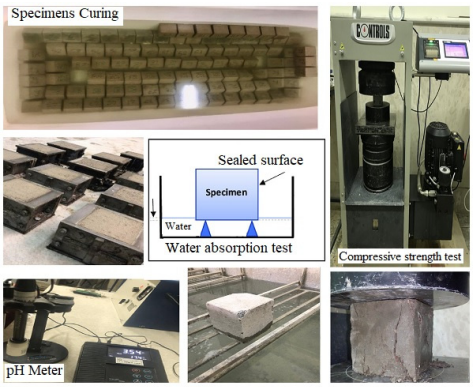

Figure 1. Test setup and preparing the specimen to perform the experimental tests.

Response surface methodology (RSM) is a statistical technique to optimize processes and systems involving multiple independent and dependent variables. In this research, a second-order polynomial equation (quadratic model) was used to model the relationship between the independent and dependent variables (e.g., silica fume and metakaolin replacement, water absorption, and compressive strength). Design–Expert Software v.11 provides a framework to implement RSM through a structured process involving problem definition, experimental design, data collection, analysis, interpretation, and model validation. This software empowers users to optimize processes and systems effectively by identifying critical variables, determining optimal settings, and predicting outcomes. Besides the primary experimental studies, the response surface methodology (RSM) was employed using Design–Expert software to determine optimum amounts of concrete mixture proportions. Considering two variables at different levels, metakaolin in five levels (0, 10, 20, 30, 40%) and silica fume in three levels (0, 5, 10%) in Design–Expert software, the optimal (Custom) part with two central points was used to determine mix-design. In this method, the distance of all levels is equal to each other and varies from −1 to +1. The final mix design can be seen in Table 2. To ensure that excess heat does not impact the alkali-activated concrete system, the alkaline-activating solution made from sodium silicate and sodium hydroxide chemicals was prepared 24 h in advance, owing to its thermogenic nature. This preparation process is recommended as per the research presented in [46,47]. After removing the molds, the specimens were water-cured for 27 days before being placed in an acidic environment. At the age of 28, after weighing, the specimens were placed in a sulfuric acid solution with pH = 1 ± 0.05 for 90 days.

Table 2. Mix design properties (kg/m^3).

Mixture	Slag	Metakaolin	Silica Fume
GGBFS	408	-	-
SF5	387.6	-	20.4
SF10	367.2	-	40.8
MK10	367.2	40.8	-
MK10SF5	346.8	40.8	20.4
MK10SF10	326.4	40.8	40.8
MK20	326.4	81.6	-
MK20SF5	306	81.6	20.4
MK20SF10	285.6	81.6	40.8

Table 2. *Cont.*

Mixture	Slag	Metakaolin	Silica Fume
MK30	285.6	122.4	-
MK30SF5	265.2	122.4	20.4
MK30SF10	244.8	122.4	40.8
MK40	244.8	163.2	-
MK40SF5	214	163.2	20.4
MK40SF10	204	163.2	40.8

3. Results and Discussion

In total, 15 mixtures were designed to study the effect of various alkali-activated binders on the durability and mechanical properties of alkali-activated concrete exposed to an acidic environment. The obtained results are presented in the following 3 groups. The first group evaluates the effects of pozzolan content on alkali-activated concrete properties after 28 days of curing. The second group measures the resistance of alkali-activated concrete to sulfuric acid attack after 90 days of exposure, and the third group analyzes the microstructure of the exposed concrete using scanning electron microscopy (SEM).

3.1. Mechanical Properties and Water Absorption

Table 3 shows the studied mix-design compressive strength and water absorption of 7 and 28 days cured concrete specimens. As indicated in Table 3, the highest 28 days' compressive strength is 63 MPa for the GGBFS mix with 100% slag, and the lowest value is 41 MPa for the MK40SF5 mixture with 40% metakaolin and 5% silica fume. According to the obtained results, adding metakaolin and silica fume reduces compressive strength in 7 and 28 days of curing in water. The compressive strength of the combined design decreased as the metakaolin and silica fume content increased. This trend is comparable to other mix designs like SF5, SF10, MK10, and MK40. In each case, slag was replaced with metakaolin or silica fume. By increasing the metakaolin and silica fume from 0% to 10% and 0% to 5%, respectively, the compressive strength reduces at a higher rate. In higher content, the compressive strength reduction rate slows down. In materials with predominantly aluminum-silicate content, increasing the amount of calcium oxide leads to the formation of structures such as hydrated calcium silicate and hydrated calcium aluminate silicate, which ultimately leads to a notable increase in the mechanical properties of concrete [48].

Table 3. The studied mix-design compressive strength and water absorption.

Mix	Compressive Strength (MPa)		Water Absorption (%)			
			Short Time		Ultimate	
	7 Days	28 Days	7 Days	28 Days	7 Days	28 Days
GGBFS	50.2	63	3.77	3.09	4.2	3.38
SF5	50.8	60	3.4	2.89	3.73	3.18
SF10	47.9	57.3	3.43	2.41	3.78	2.78
MK10	39.7	55.5	3.99	3.43	4.47	3.82
MK10SF5	37.4	49.8	4.01	3.37	4.41	3.59
MK10SF10	34.4	47.1	3.68	3.11	4.01	3.41
MK20	35.4	50.1	4.39	3.73	4.78	4.14
MK20SF5	31.8	44	3.96	3.26	4.36	3.66
MK20SF10	31.2	43.5	3.78	3.11	4.18	3.45
MK30	32.3	47.3	4.54	3.89	4.96	4.31
MK30SF5	29.8	42.6	4.31	3.71	4.79	4.09
MK30SF10	29.8	42.4	4.05	3.41	4.42	3.63
MK40	30.7	45.4	4.66	3.96	5.1	4.32
MK40SF5	28.9	41	4.41	3.81	4.98	4.14
MK40SF10	30	41.9	3.95	3.39	4.38	3.68

The short-term and final water absorption amounts are presented in Table 3 regarding the metakaolin content and silica fume replacement. As indicated, the short-term and final water absorption decreased with increasing silica fume. At 28-day ages, when 5% and 10% of silica fume were used as replacements, the short-term water absorption decreased by 6.5% and 22%, respectively. In addition, the final water absorption was reduced by 5.9% and 17.8% compared to mixes without silica fume. Therefore, increasing the silica fume reduces the voids between the slag grains and the gel, reducing water absorption. Silica fume in concrete densifies its microstructure due to small particle size and participates in chemical reactions, leading to the deposition of hardened products, which significantly reduces permeability [22].

According to Table 3, metakaolin not only did not have a positive effect, but its increase affected short-term and final water absorption negatively. In fact, with the increase of metakaolin content up to 40%, the rate of short-term and final water absorption has increased significantly compared to the GGBFS mix design in 28-day ages. Meanwhile, the laboratory results show that adding silica fume up to 10% to alkali-active concrete with up to 40% metakaolin content always reduces the initial and final water absorption.

3.1.1. Compressive Strength

The influence of silica fume replacement on the compressive strength of AAS concrete has been shown in Figure 2a. Due to the filler effect, 5% silica fume replacement slightly improves compressive strength at the age of 7 days. But increasing silica fume replacement by up to 10% has reduced the 7-day strength by 4.5%. Meanwhile, 5% and 10% of SF replacement values have reduced the 28-day compressive strength. Figure 2b. shows the effect of metakaolin replacement on the compressive strength of AAS concrete at the ages of 7 and 28 days. In 10, 20, 30, and 40% replacement, the compressive strength of 7 and 28 days has decreased continuously. At the highest amount of replacement (40% MK), the compressive strength of AAS concrete at the ages of 7 and 28 days decreased by 38.8% and 27.9%, respectively. Figure 2c also shows the interaction of silica fume and metakaolin replacement on AAS concrete's compressive strength at 28 days. According to the illustration, incorporating metakaolin as a replacement in AAS concrete results in a decline in compressive strength. Moreover, replacing 5% or 10% of the AAS concrete with silica fume when metakaolin replaces up to 40% of slag reduces compressive strength. The decrease in the strength of specimens containing metakaolin and silica fume is attributed to the reduction of calcium oxide content, as an affecting factor on concrete mechanical properties and lack of thermal treatment, which is necessary for gaining strength in calcium oxide-free alumino-silicate precursor [49,50].

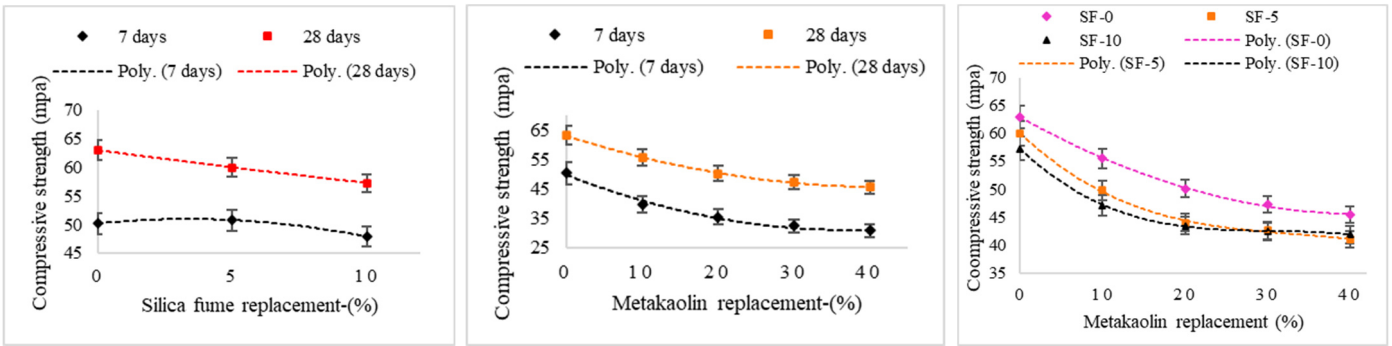

(**a**) (**b**) (**c**)

Figure 2. (**a**) Effect of silica fume replacement on compressive strength, (**b**) Effect of metakaolin replacement on compressive strength, (**c**) Interaction of SF and MK on compressive strength.

In Figure 3, 3D response surface models and 2D contour lines are plotted graphically for compressive strength. The 3D response surface models (Figure 3a) show that adding metakaolin and silica fume to the alkali-activated slag concrete mixture reduces compressive

strength. The yellow and red regions in the 2D contour lines (Figure 3b) display the combination resulting in the optimal compressive strength. It is worth noting that about 90% of the metakaolin mass consists of silicon and aluminum oxides, and more than 96% of silica fume content is silicon oxide. Therefore, replacing slag, which contains large amounts of CaO, with these materials has caused a reduction in compressive strength, which has consistency with other scientific reports [51–53].

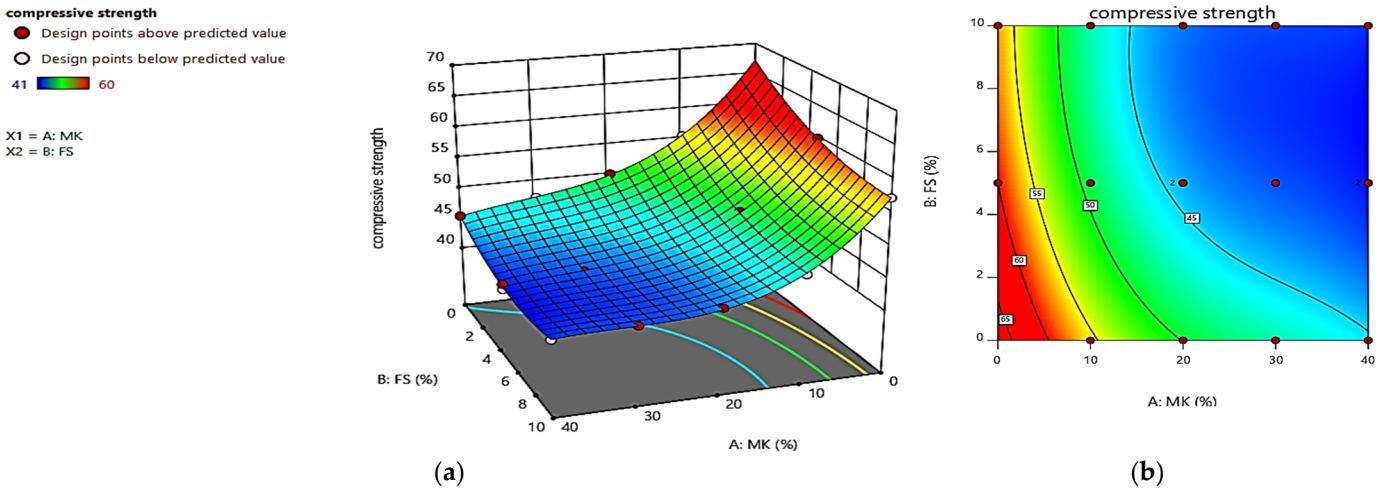

Figure 3. (**a**) 3-D response surface models for compressive strength (**b**) 2-D contour plot.

3.1.2. Reduction in Compressive Strength

In this section, the compressive strength test results of alkali-activated slag concrete were kept exposed to sulfuric acid pH = 1 ± 0.05, and the effect of replacement and increase of metakaolin and silica fume on the compressive strength of alkali-activated slag concrete are discussed. Figure 4a shows the reduction values in compressive strength of alkali-activated concrete and the effect of slag replacement with different silica fume contents at different exposure times. Increasing silica fume and replacing it has improved the performance and recovered the concrete compressive strength reduction, so that after 90 days of exposure time, the highest reduction in compressive strength (19.1%) was related to GGBFS specimens, and the lowest reduction in compressive strength (11.1%) was related to the SF10 mix-design, which has the highest amount of slag content replacement with silica fume. By replacing 5% and 10% of silica fume with slag in AAS concrete, the loss of compressive strength owing to acid attack was reduced by 57% and 72% after 30 days, 25% and 55% after 60 days, and 30% and 41% after 90 days.

Figure 4b shows the compressive strength reduction of alkali-activated slag concrete and the effect of slag replacement with different metakaolin contents at different ages after exposure to sulfuric acid at pH = 1 ± 0.05. Increasing metakaolin and replacing it has initially caused an increase in compressive strength reduction. So that after 90 days, exposure of specimens containing 10% metakaolin to acid increased the compressive strength reduction to 1.6% compared to the control specimens. Due to the high content of slag in the specimens, which contains a significant amount of calcium oxide, and the porous nature of the geopolymer surface (N-A-S-H) compared to the surface containing calcium (C-S-H), the addition of 10% metakaolin resulted in the formation of cavities and pores on the concrete surface. This reaction caused more acid to penetrate the specimens, react with $Ca(OH)_2$ due to the hydration of the slag, and produce gypsum as a white, low-strength substance. Therefore, the compressive strength of the specimens was reduced more than the control specimens. Increasing slag replacement by 20% and 30% of metakaolin has improved performance and reduced compressive strength decline. So, after 90 days of exposure time, the highest reduction in compressive strength (19.1% and 20.1%) is related

to the specimens containing 100% slag and the specimens containing 10% metakaolin and the lowest compressive strength reduction (8.3%), belonged to the specimens with the highest content of slag (40%) replaced with metakaolin.

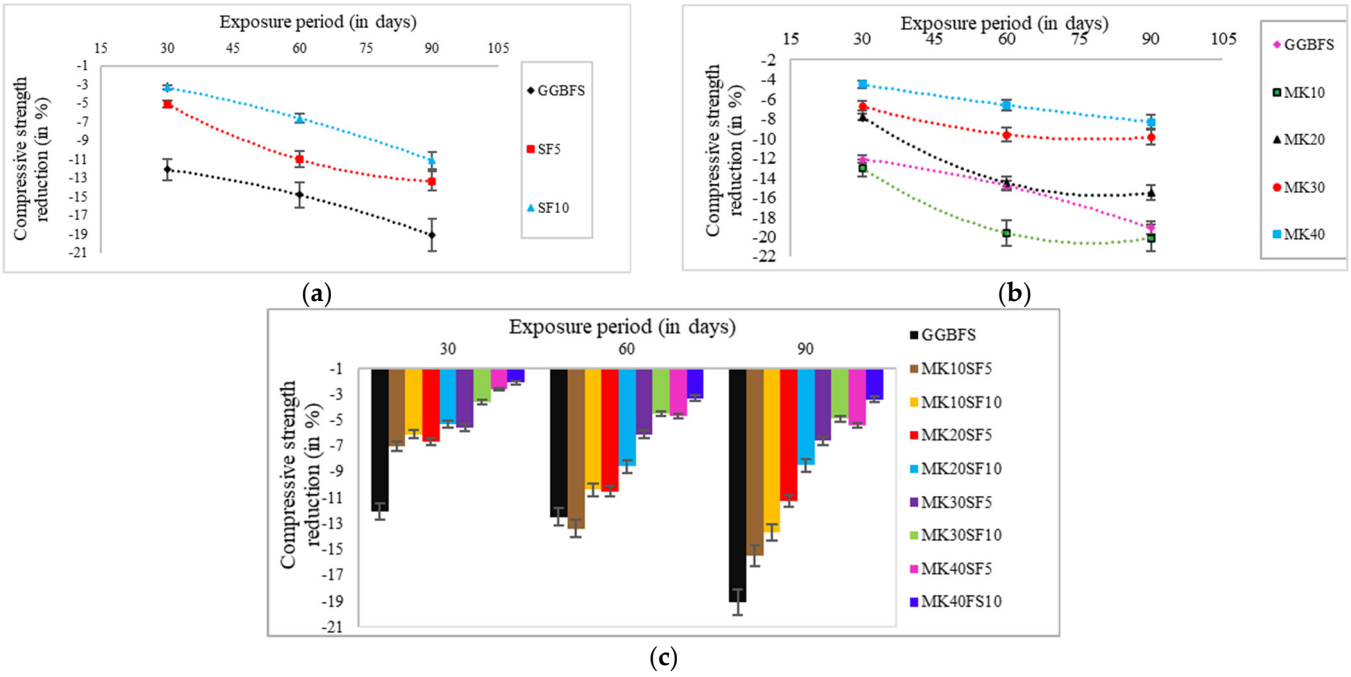

Figure 4. Compressive strength reduction during sulfuric acid exposure in alkali activated concrete specimens (**a**) containing 0, 5 & 10% SF, (**b**) containing 0, 10, 20 & 30% MK, (**c**) containing percentages of both MK and SF.

It can be seen in Figure 4c that increasing the metakaolin content in the mix designs from 0 to 40% and the silica content from 0 to 10% has improved the reduction in compressive strength. So, the mix with slag and its replacement with 40% metakaolin and 10% silica fume had a considerably strong performance in sulfuric acid. In this mix, after 90 days of exposure to sulfuric acid, there was only a 3.4% reduction in compressive strength compared to 28-day compressive strength.

Figure 5 indicates the interaction between the relevant variables graphically. The results show that the slag-based mix design with the replacement of 40% metakaolin and 10% silica fume has the least reduction in compressive strength after 90 days in an acid solution. The highest reduction in compressive strength is during the first 30 days of exposure time. It can be concluded that because the alkalinity of the mixes is high due to sodium hydroxide and sodium silicate, by being placed in an acidic solution, the specimens reacted more with sulfuric acid in the early ages, and this has led to a reduction in the compressive strength. Although increasing the slag increased the 28-day compressive strength of the specimens, it did not considerably affect the process of reducing the compressive strength in the sulfuric acid solution. Therefore, although increasing metakaolin and silica fume reduces the 28-day compressive strength of alkali-activated slag concrete, this has led to improved performance against sulfuric acid. As mentioned, calcium hydroxide and C-S-H decompose in contact with corrosive and invasive environments, including acids. Therefore, replacing metakaolin and silica fume with slag, which contains large amounts of CaO as the main factor in the production of calcium hydroxide, has improved the performance of specimens under sulfuric acid. Thus, it can be concluded that the chemical attack is more influenced by the nature of the hydration products of the binder than the degree of porosity.

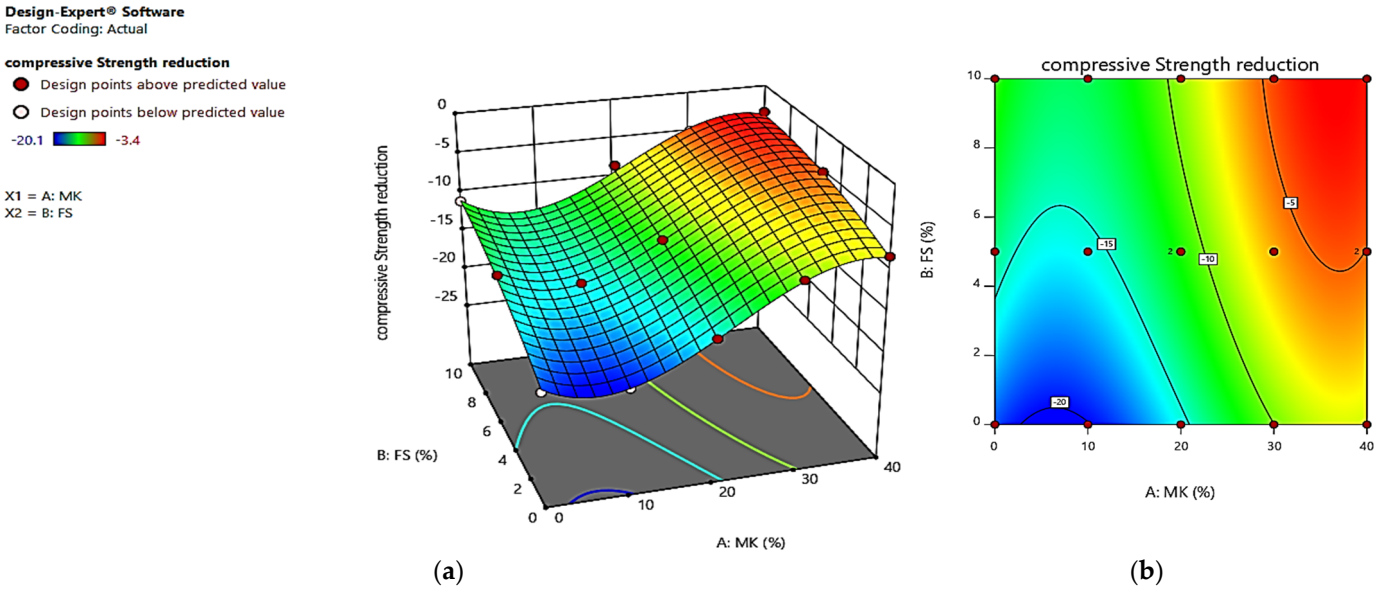

Figure 5. Response surface diagrams for compressive Strength reduction (**a**) 3-D response surface model (**b**) 2-D contour plot.

The short-term and final water absorption diagrams, as the important factors determining the concrete durability, are illustrated in Figure 6a,b regarding the silica fume content and metakaolin replacement, respectively. The influence of silica fume replacement on 7 days and 28 days ultimate water absorption of AAS concrete has been shown in Figure 6a. 5% silica fume replacement in AAS concrete decreased 11% of water absorption at the age of 7 days, which shows the filler effect of silica fume. But increasing the replacement of silica fume up to 10% has not significantly affected water absorption compared to SF5 at the age of 7 days. Meanwhile, 5 and 10% of SF replacement values have relatively consistently reduced the 28-day water absorption up to 27%. Figure 6b shows the effect of metakaolin replacement on water absorption of AAS concrete at the ages of 7 and 28 days. In replacing slag with 10, 20, 30, and 40% metakaolin, with the increase of the replacement, the water absorption of 7 and 28 days has increased continuously. At the highest amount of replacement (40% MK), the water absorption of AAS concrete at the ages of 7 and 28 days increased by 21% and 12%, respectively. Figure 6c also shows the interaction of silica fume and metakaolin replacement on the ultimate water absorption of AAS concrete at 28 days. The figure shows that in addition to the replacement of metakaolin in AAS concrete increasing the water absorption, the replacement of 5% and 10% silica fume to the AAS concrete where a part of the slag (up to 40%) is replaced by metakaolin also decreases the water absorption.

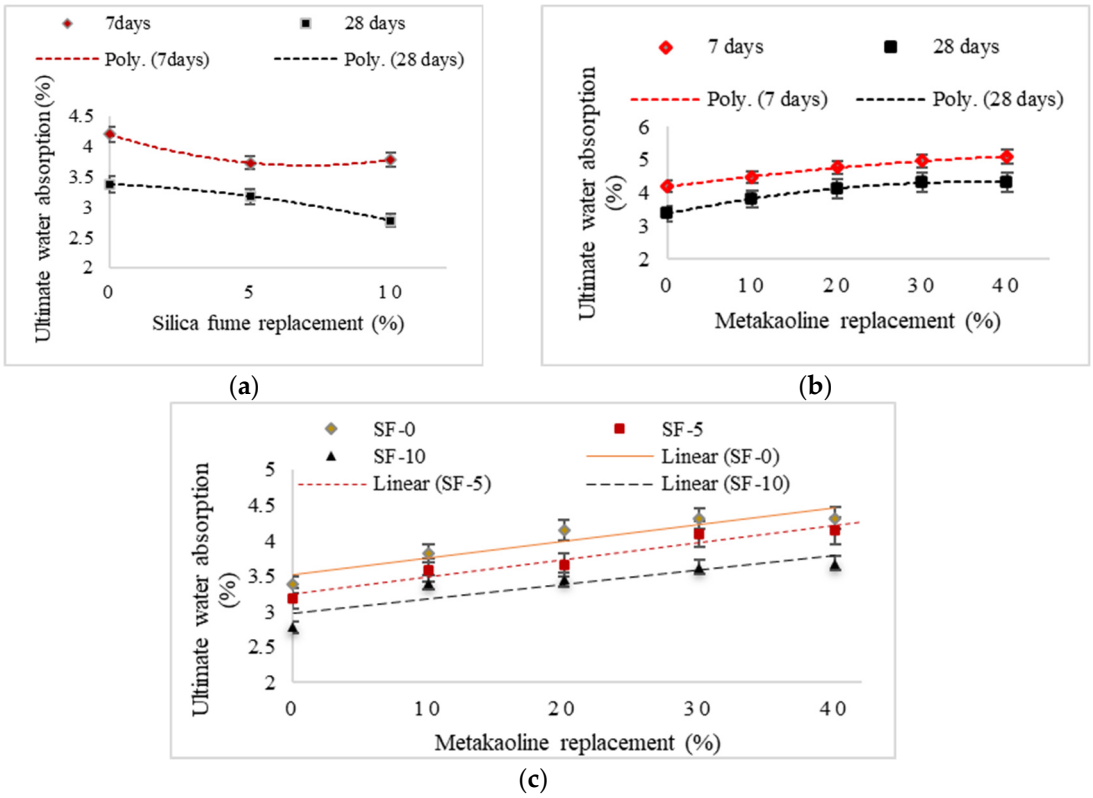

Figure 6. (**a**) Effect of SF replacement on water absorption, (**b**) Effect of MK replacement on water absorption, (**c**) Interaction of SF and MK on water absorption.

In the mix-design containing metakaolin and silica fume, short-term and final water absorption increased compared to the control specimens (GGBFS). According to Figure 6, comparing short-term and final water absorption of 7 days and 28 days, 28-day tests had less water absorption in all cases. According to Figure 7, the highest final water absorption of the 28-day specimen is related to the MK40 mix design, with the highest slag content with metakaolin. Geopolymer concrete is formed simultaneously with alkali-activated concrete by adding metakaolin and slag. As a result, the cavities and pores inside the geopolymer concrete increase the short-term and final water absorption.

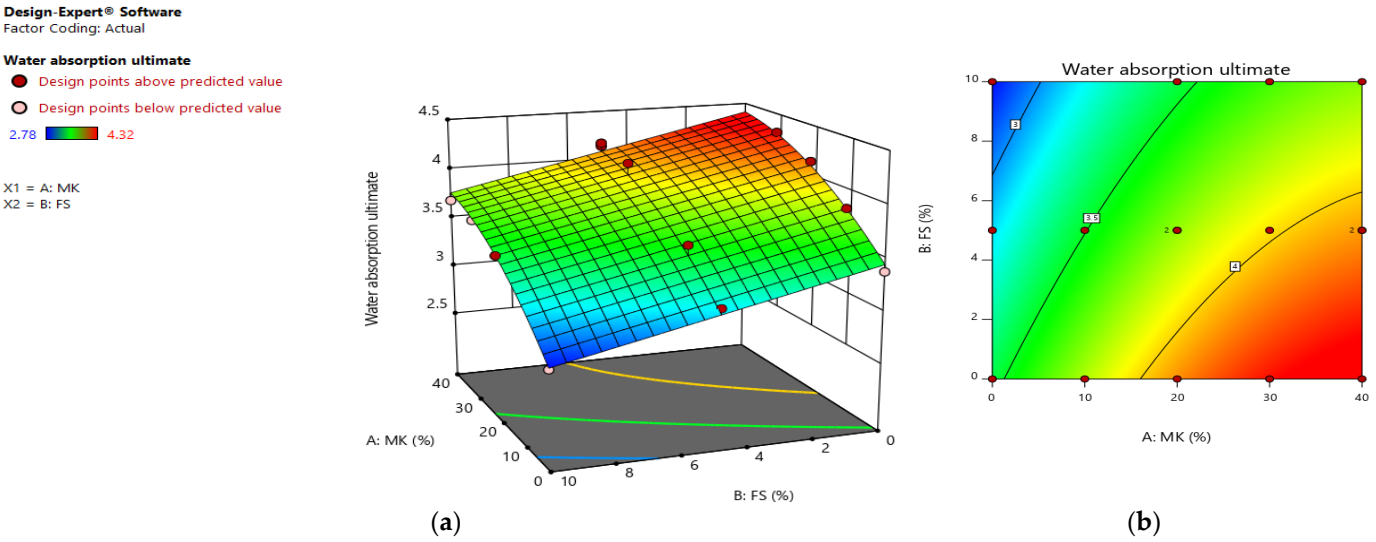

Figure 7. Response surface diagrams for water absorption (**a**) 3-D response surface model (**b**) 2-D contour plot.

The short-term and final water absorptions of a concrete sample refer to the amount of water that the concrete absorbs within the first few hours and a specific period of time, respectively. On the other hand, capillary water absorption pertains to the concrete's water absorption rate over time. Considering the impact of this factor on concrete durability, capillary water absorption and its rate in 7-day and 28-day specimens are investigated, and results are depicted in Table 4. As shown, adding silica fume to the mixtures reduces the 3 h initial rate of absorption "i" and capillary absorptivity coefficient "S" of 28 days compared to GGBFS specimens. "i" ($gr/cm^2.min$) indicates the speed of water penetration from the surface to the inside of concrete, while "S" (gr/cm^2) shows the final amount of water absorbed. An increase in "i" and "S" speeds up penetration and reduces the durability of the concrete structure. As shown in Table 4, although specimens with silica fume had a higher absorption rate than the control ones (GGBFS) in the early hours, at the end of the test, the water absorption of the control specimen (GGBFS) was more than the specimens with silica fume. The mixtures containing metakaolin showed a higher capillary water absorption than the GGBFS specimens in 7 and 28 days. This is due to the large surface area and plate-shaped particles of metakaolin and the high demand for water in this type of concrete [34].

Table 4. Capillary water absorption of cast alkali-activated at the age of 7 days.

Mix Design	7 Days ($\times 10^{-2}$) Gr				i ($\times 10^{-3}$) Gr/cm^2 /min	S Gr/cm^2	28 Days ($\times 10^{-2}$) Gr				i ($\times 10^{-3}$) Gr/cm^2 /min	S Gr/cm^2
	3 h	6 h	24 h	72 h			3 h	6 h	24 h	72 h		
GGBFS	10,150	11,150	11,750	11,325	5.63	1.13	4575	6800	8050	8775	2.54	0.87
SF5	10,000	10,200	10,425	10,650	5.55	1.06	4500	6000	6250	6475	2.50	0.64
SF10	9600	9800	10,000	10,150	5.33	1.01	4800	6700	7050	7175	2.66	0.71
MK10	9400	10,550	11,450	11,525	5.22	1.15	4900	6950	8750	9250	2.72	0.92
MK10SF5	10,900	11,750	11,850	11,900	6.05	1.19	6225	8500	8650	8800	3.45	0.88
MK10SF10	11,000	11,300	11,400	11,400	6.11	1.14	6025	8850	9300	9450	3.34	0.94
MK20	10,850	11,275	11,400	11,500	6.02	1.15	6050	9150	9500	9675	3.36	0.96
MK20SF5	10,550	11,300	11,600	11,700	5.86	1.17	6450	8800	9050	9200	3.58	0.92
MK20SF10	11,150	11,300	11,400	11,450	6.19	1.14	5700	7900	8250	8500	3.16	0.85
MK30	11,600	11,750	11,950	12,000	6.44	1.20	6275	6375	9700	9850	3.48	0.98
MK30SF5	10,800	11,100	11,300	11,450	6.00	1.14	5775	8550	8775	9000	3.20	0.90
MK30SF10	10,875	11,300	11,450	11,650	6.04	1.16	6150	9150	9275	9375	3.41	0.937
MK40	10,950	11,375	11,775	11,950	6.08	1.19	6250	9150	9375	9650	3.47	0.96
MK40SF5	10,675	11,100	11,350	11,500	5.93	1.15	5775	8675	8800	9300	3.20	0.93
MK40SF10	10,750	11,150	11,400	11,600	5.97	1.16	5900	8850	8950	9175	3.27	0.91

3.2. Mass Changes

Figure 8 indicates the mass changes due to sulfuric acid for alkali-activated slag concrete containing different metakaolin and silica fume content compared to the GGBFS. The results were normalized based on the weight gain of the GGBFS mix design. As illustrated, all specimens experienced increased mass at all ages after exposure to the sulfuric acid solution. In this regard, the GGBFS had a 2.31% increased mass after 90 days in the acid pool, and specimens containing 10%, 20%, 30%, and 40% metakaolin experienced a mass increase of 1.91%, 1.36%, 1.34%, and 1.29%, respectively. Increasing the slag content replacement with metakaolin reduced this weight gain compared to the GGBFS mix design. According to Figure 8, replacing slag with silica fume also increases the specimen's mass. However, the weight gains of the silica fume mixes were less than the GGBFS mix design. Furthermore, it has been observed that the mixes containing metakaolin and silica fume have a lower mass gain even after being exposed for 30, 60, and 90 days, compared to other combinations.

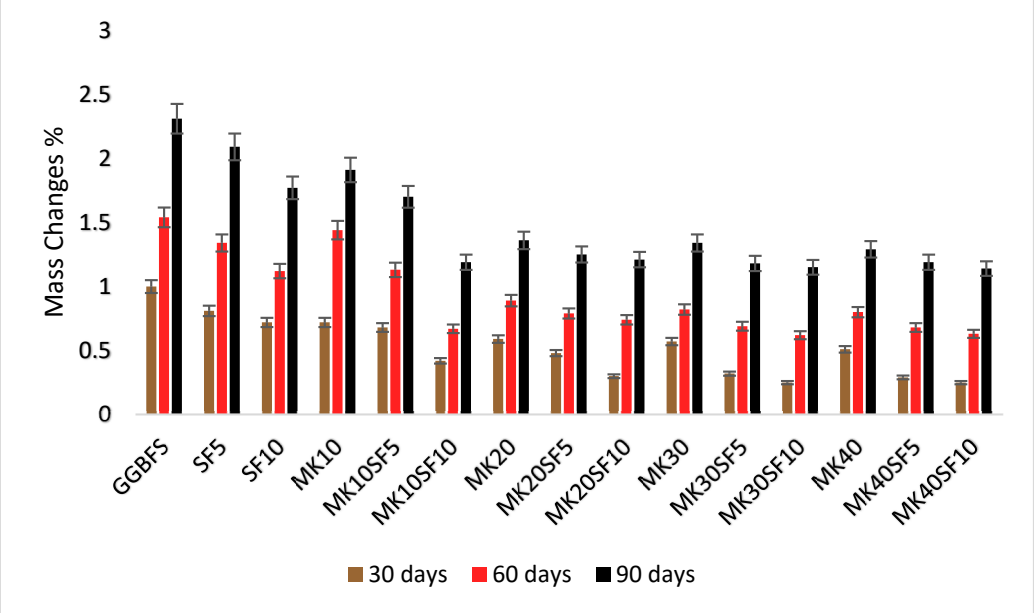

Figure 8. Normalized mass change of alkali-activated concrete specimens exposed to sulfuric acid solution.

The increase in weight of the specimens immersed in the acid pool is a result of the reaction between $Ca(OH)_2$ and acid. This reaction leads to the accumulation of a thin layer of calcium sulfate and calcium sulfoaluminate on the surface of the concrete. The permeable anions of SO_4^{2-} interact with calcium ions, leading to the formation of gypsum crystals and a subsequent increase in the weight of the concrete specimens [35]. Replacing metakaolin and silica fume with slag, which contains large amounts of CaO as the primary source of mass gain in reaction with acid, has reduced the mass gain owing to the cited process. This is so that the specimens with 40% metakaolin and 10% silica fume after 90 days of exposure had the least mass gain compared to other mixtures.

3.3. SEM and EDS Test Results

Scanning electron microscopy (SEM) and energy-dispersive X-ray spectroscopy (EDS) are valuable techniques for characterizing alkali activated binder's (AAB) microstructure and elemental composition. SEM provides high-resolution images of the material's surface, enabling the study of pore morphology, gel particle distribution, and unreacted precursors. EDS, on the other hand, quantifies the relative abundances of elements present in the material, allowing for the identification of phases, analysis of gel particle formation, and investigation of different condition effects on microstructure. In this investigation, these insights gained from SEM/EDS analysis contribute to a deeper understanding of AAB properties and the development of optimized AA materials. Figure 9 shows a scanning electron microscopy (SEM) image at a scale of 100 µm to study the microstructure of alkali-activated slag concrete containing metakaolin and silica fume after 28 days of curing.

This microscopic image shows the microstructural features of two separate systems and phases formed, geopolymer concrete and active alkali concrete, within the adhesive. The two phases formed in this concrete result from slag and metakaolin usage in the adhesive composition. The results of energy-dispersive spectroscopy (EDS) analysis taken from phases A and B are shown in Figure 10, which shows that the most significant difference in the constituents of these two phases is in the amounts of calcium and silicon.

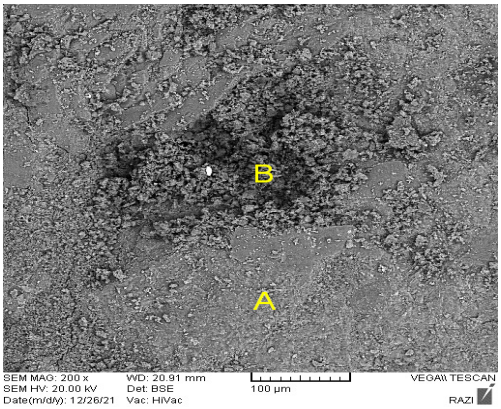

Figure 9. SEM micrograph of matrix MK40 (60% slag, 40% Metakaolin) at 28 days. Identification of the different phases: (A) geopolymer binder with low calcium content; (B) calcium silicate hydrate with a small proportion of aluminum.

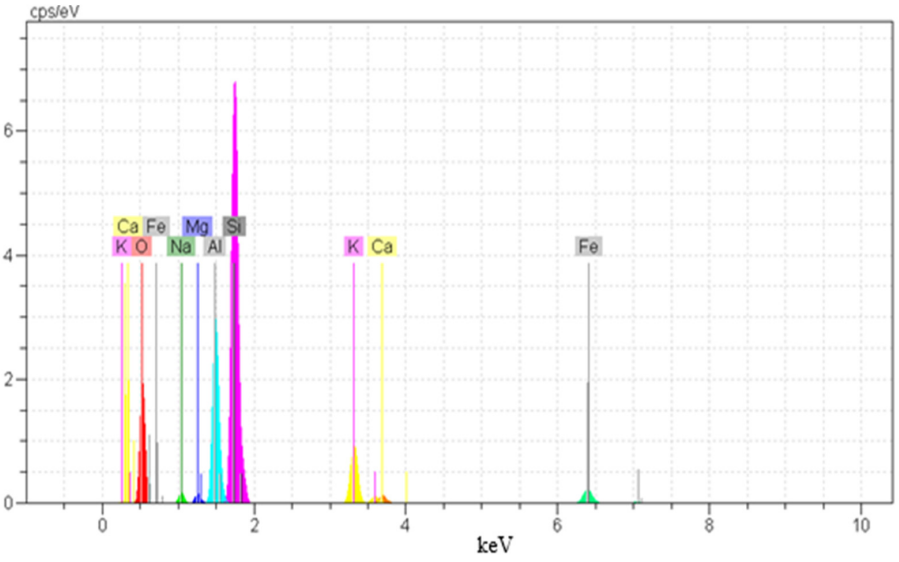

(**a**)

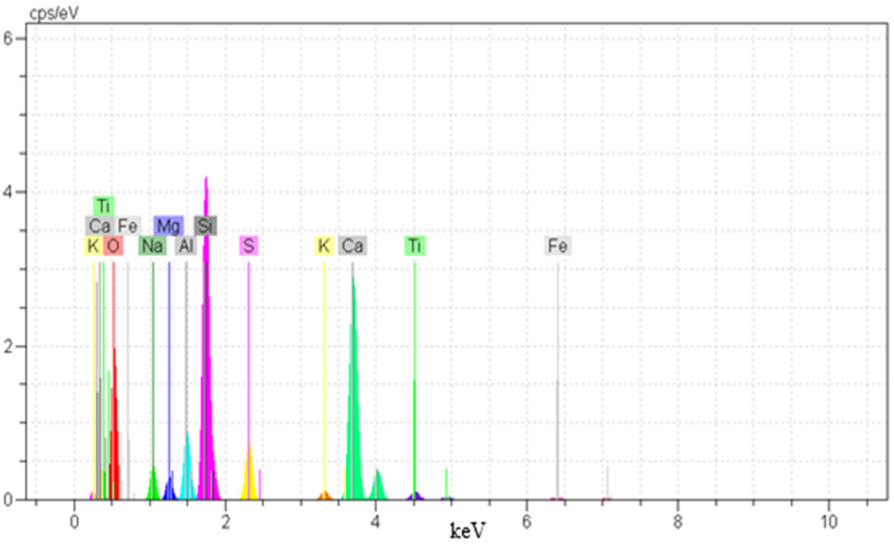

(**b**)

Figure 10. EDS analysis results of (**a**): phase A and (**b**) phase B of concrete (shown in Figure 9).

EDS analysis (Table 5) found that the concrete composition in zone A is composed of silicon, aluminum, sodium, and less than 1% by weight of calcium due to the addition of metakaolin in the system. At the same time, the B area is composed of silicon and calcium from the slag and with a small amount of aluminate and sodium. The EDS spectra for phase B show peaks corresponding to both Si and Ca (Figure 10). This further confirms the presence of these elements in phase B and indicates that they are forming a chemical bond. The relative concentrations of Si and Ca in phase B are consistent with a Ca-Si compound. The EDS data shows that phase B's Si to Ca ratio is approximately 1:1, consistent with the stoichiometry of calcium silicate ($CaSiO_3$), the most stable calcium silicate compound under experimental conditions.

Table 5. The average elemental compositions of phases A and B as shown in Figure 9.

	Oxygen (O)	Sodium (Na)	Aluminum (Al)	Silicon (Si)	Calcium (Ca)	Magnesium (Mg)	Sulfur (S)	Potassium (K)	Titanium (Ti)	Iron (Fe)
					%					
Phase A	53.08	0.91	10.75	25.83	0.63	0.61	-	5.09	-	3.11
Phase B	56.40	2.79	3.66	16.25	14.8	1.4	2.91	0.5	0.87	0.39

Figure 11 shows the product of Zone A at scales of 2 and 10 µm, which has properties similar to low-calcium or calcium-free systems and can be considered a geopolymer. In Figure 11, the formation of C-S-H gel cannot be clearly seen; only small calcium deposits are partially scattered in this part of the area. A clear formation of the C-S-H phase could not be observed in such a binder; instead, scattered small calcium precipitates (the bright white islands mentioned by arrow, 20 Å width) within the binder were observed. Geopolymers based on low-calcium materials such as metakaolin tend to form N-A-S-H gels with interconnected and irregularly zeolite-type structures. Figure 11a,b shows the microstructure of the mix MK40, where there are thinner cracks and micro cracks, but in the mix MK40SF10, Figure 11c,d shows a denser matrix but with fewer and wider cracks.

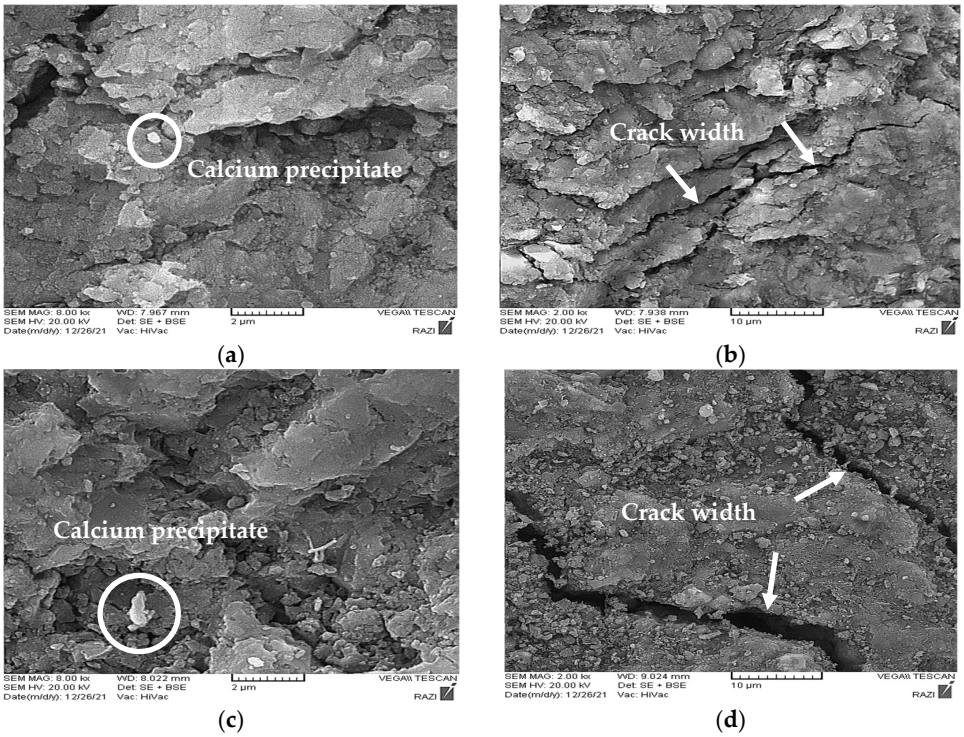

Figure 11. SEM images of (**a**,**b**) Matrix MK40 (60% slag, 40% Metakaolin) and (**c**,**d**) Matrix MK40SF10 (50% slag, 40% Metakaolin, Silica fume 10%), mixtures.

Figure 12 shows the microstructure of zone B at scales of 2 and 10 µm by Figure 12a,b and Figure 12c,d, respectively. In Figure 12a,b, the microstructure of the GGBFS matrix reveals the presence of slag particles, porous surfaces, and coarse hardened particles. On the other hand, Figure 12c,d illustrates the SF10 matrix, displaying fine round silica fume particles and higher density. This shows that more compaction led to less penetration of the attacking fluid. Still, since the harder particles of hydrated slag provide more strength by creating more internal friction, the compressive strength and water absorption of GGBFS are higher than SF10. It can be seen that there is a significant correlation and relationship between the apparent observations using scanning electron microscopy and the results of the experiments of this research.

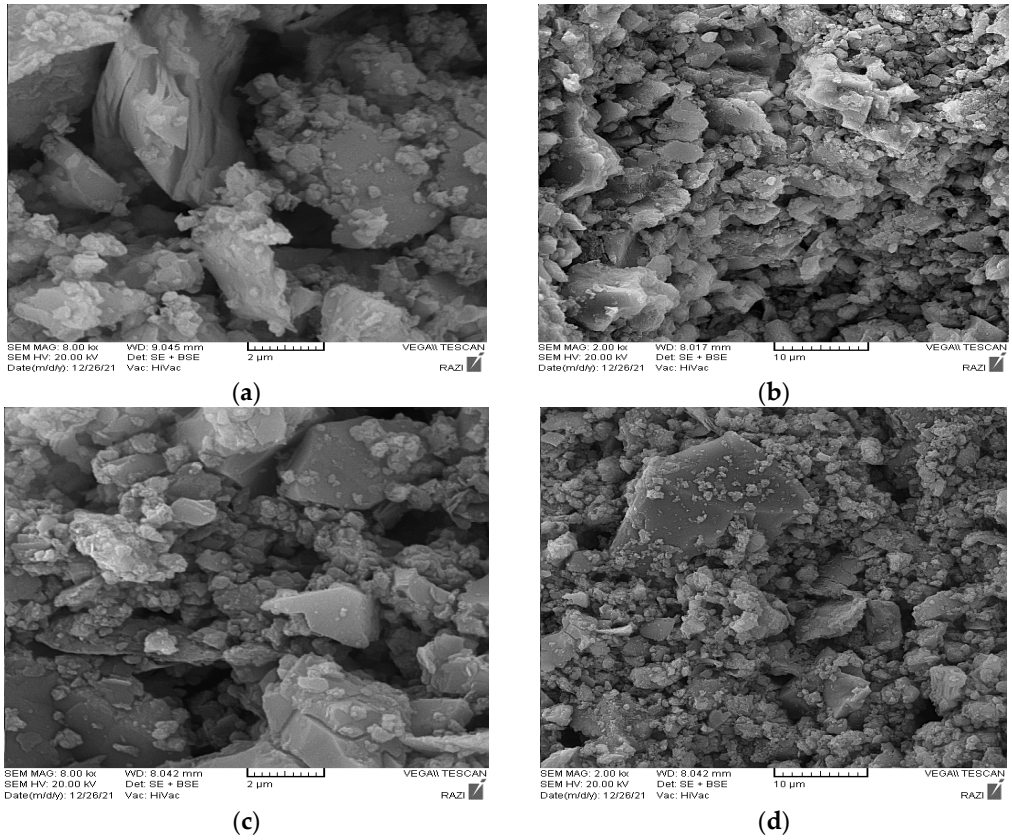

Figure 12. SEM images of (**a**,**b**) Matrix GGBFS (100% slag) and (**c**,**d**) Matrix SF10 (90% slag, Silica fume 10%).

Combining high-calcium raw materials like blast furnace slag with alkalis such as sodium hydroxide produces calcium silicate hydrate gel (C-S-H) products with varying Ca to Si ratios. The C-S-H gel produced through this process has a much lower Ca–Si ratio than the one formed during conventional Portland cement hydration, as stated in [54]. According to Taylor [15], in active alkali cement, this ratio is less than 1.5 and up to 0.8, while in ordinary Portland cement, this ratio is approximately 1.8 to 2. Analyzing scan electron microscopy (SEM) images showed that adding slag to the system significantly improved the compressive strength in the structure of the geopolymer gel with the formation of hydrated calcium silicate. By comparing Figures 11 and 12, it can be concluded that the geopolymer concrete has more cavities and micro-cracks compared to the calcium-containing concrete, which has reduced the compressive strength of specimens containing metakaolin. The images show a high correlation between SEM and compressive strength results of active alkali concrete specimens.

3.4. Statistical Interpretation of Test Results

In this section, the results obtained from the compressive strength test, the reduction of compressive strength after immersion of the specimens in sulfuric acid, and the final water absorption were statistically analyzed by Design–Expert software. At first, this method was used only to find the relationship between the response and the input variables. Then, it was used to do the optimization as well. The variables include the components of the concrete mix design, and the responses are the desired concrete properties. According to Table 6, input variables A and B are defined as the slag replacement values with metakaolin (MK) and silica fume (SF). These two were considered independent variables with two central points in the form of 17 runs. Compressive strength, reduction of compressive strength, and final water absorption are interdependent responses.

Table 6. Experimental design matrix and results.

RUN	Factor 1 A:MK	Factor 2 B:SF	Response 1 Compressive Strength (MPa)		Response 2 Compressive Strength Reduction (%)		Response 3 Water Absorption (Ultimate) (%)	
	%	%	Actual Value	Predicted Value	Actual Value	Predicted Value	Actual Value	Predicted Value
1	40	0	45.4	45.36	−8.3	−8.44	4.32	4.41
2	0	5	60	59.99	−13.3	−13.87	3.18	3.12
3	10	5	49.5	49.19	−15.5	−15.56	3.59	3.49
4	10	10	47.1	47.32	−13.7	−13.08	3.41	3.16
5	20	5	44.2	44.29	−11.5	−11.39	3.7	3.78
6	20	10	43.5	43.24	−8.5	−9.29	3.45	3.45
7	10	0	55.5	55.63	−20.1	−20.09	3.82	3.82
8	0	10	57.3	57.3	−11.1	−11.00	2.78	2.79
9	40	5	41	41.38	−5	−5.05	4.17	4.08
10	30	10	42.4	42.36	−4.9	−4.53	3.63	3.65
11	30	0	47.3	47.39	−9.87	−10.02	4.31	4.30
12	40	10	41.9	41.97	−3.4	−3.71	3.68	3.76
13	20	0	50.1	49.91	−15.5	−15.54	4.14	4.10
14	40	5	41.8	41.38	−5.4	−5.05	4.14	4.08
15	20	5	44	44.29	−11.27	−11.39	3.66	3.78
16	30	5	42.6	42.59	−6.6	−6.25	4.09	3.97
17	0	0	63	64.48	−19.1	−18.78	3.38	3.45

As shown in Table 7, the Cubic model is used for the compressive strength responses, and the compressive strength reduction and the Quadratic model was used for the final water absorption response. In Table 7, F and *p*-values indicate disproportion and dispersion of the data, respectively. Variables whose *p*-value is less than 0.05 indicate that the term is significant. In contrast, the software removes variables with a *p*-value more than 0.05 as they are known as insignificant, which may even increase the error in the computation process. The *p*-value was considered for the following factors: GGBFS replacement with MK (A), GGBFS replacement with SF (B), multiply the MK and the SF replacement (AB), quadratic power of replacement percentage of MK (A^2), the second power of the SF (B^2) replacement and the third power of the MK (A^3) replacement in the optimal production of compressive strength reduction after immersion and their effect on the compressive strength equation (Equation (1)). The equations of three responses, compressive strength, reduction of compressive strength, and final water absorption after 90 days' exposure, have been summarized in following:

$$\text{Compressive strength} = 44.29 - 5.7A - 3.34B + 1.64AB + 6.39A^2 + 2.29B^2 - 3.61A^3 \quad (1)$$

$$\text{Compressive strength reduction} = -11.39 + 10.94A + 3.13B - 0.7630AB + 1.94A^2 - 1.02B^2 - 6.54A^3 \quad (2)$$

$$\text{Water absorption} = 3.78 + 0.4817A - 0.3264B - 0.1735A^2 \quad (3)$$

Table 7. Anova response models.

Responses	Source	Sum of Squares	df	Mean Square	F-Value	*p*-Value	
Compressive strength (MPa)	Model	523.68	8	65.46	672.94	<0.0001	significant
	A-Mt	19.55	1	19.65	200.97	<0.0001	
	B-Sf	42.62	1	42.62	438.15	<0.0001	
	AB	5.58	1	5.58	57.32	0.0001	
	A^2	77.10	1	77.10	792.59	<0.0001	
	B^2	16.81	1	16.81	172.82	<0.0001	
	A^2B	0.0046	1	0.0046	0.0475	0.8337	
	AB^2	0.0033	1	0.0033	0.0340	0.8590	
	A^3	7.10	1	7.10	72.97	<0.0001	
	B^3	0.0000	0				
	Residual	0.6809	7	0.0973			
	Lack of Fit	0.3409	5	0.0682	0.4011	0.8226	not significant
	Pure Error	0.3400	2	0.1700			
	Cor Total	524.36	15				
Compressive strength reduction (%)	Model	396.01	8	49.50	282.24	<0.0001	significant
	A-Mt	77.31	1	77.31	440.81	<0.0001	
	B-Sf	39.48	1	39.48	225.07	<0.0001	
	AB	2.91	1	2.91	16.60	0.0036	
	A^2	12.02	1	12.02	68.55	<0.0001	
	B^2	4.57	1	4.57	26.04	0.0009	
	A^2B	0.0066	1	0.0066	0.0377	0.8510	
	AB^2	0.5826	1	0.5826	3.32	0.1058	
	A^3	28.91	1	28.91	164.81	<0.0001	
	B^3	0.0000	0				
	Residual	1.40	8	0.1754			
	Lack of Fit	1.30	6	0.2161	4.06	0.2108	not significant
	Pure Error	0.1065	2	0.0532			
	Cor Total	397.42	16				
Water absorption ultimate (%)	Model	2.72	5	0.5447	84.58	<0.0001	significant
	A-Mt	1.83	1	1.83	284.64	<0.0001	
	B-Sf	0.9453	1	0.9453	146.80	<0.0001	
	AB	0.0003	1	0.0003	0.0517	0.8247	
	A^2	0.0890	1	0.0890	13.81	0.0040	
	B^2	0.0122	1	0.0122	1.90	0.1981	
	Residual	0.0644	10	0.0064			
	Lack of Fit	0.0631	8	0.0079	12.63	0.0754	not significant
	Pure Error	0.0013	2	0.0006			
	Cor Total	2.79	15				
	Model	2.72	5	0.5447	84.58	<0.0001	significant
	A-Mt	1.83	1	1.83	284.64	<0.0001	
	B-Sf	0.9453	1	0.9453	146.80	<0.0001	
	AB	0.0003	1	0.0003	0.0517	0.8247	

R^2 (R-Squared) detection coefficient indicates the compliance of laboratory data and the values predicted by the proposed model. As shown in Table 8, the high values of R^2 for the compressive strength (0.9987), the reduction of the compressive strength (0.9950), and the final water absorption (0.9723) indicate a reasonable overlap of the laboratory data and the predicted values. Also, the Adjusted R^2 is appropriate considering that its value is more than 0.8 in all answers, and its difference with predicted R^2 in all answers is less than 0.2, which shows the strength of this model for predicting the results. Considering that in Table 8, adequate precision of all answers has accuracy values greater than 40, which indicates the robustness of the model for use in industrial work. The standard probability plot is a graphical technique for assessing whether or not a data set is approximately normally distributed. The data are plotted against a theoretical normal distribution so that

the points should form an approximately straight line [55]. As shown in Figure 13a–c, the points are distributed around a straight line in all responses. Figure 13d–f also shows the predicted values around the experimental values. Less distance to the centerline at these points indicates a high correlation between the experimental results and the predicted values, which show strong correlations of collected results.

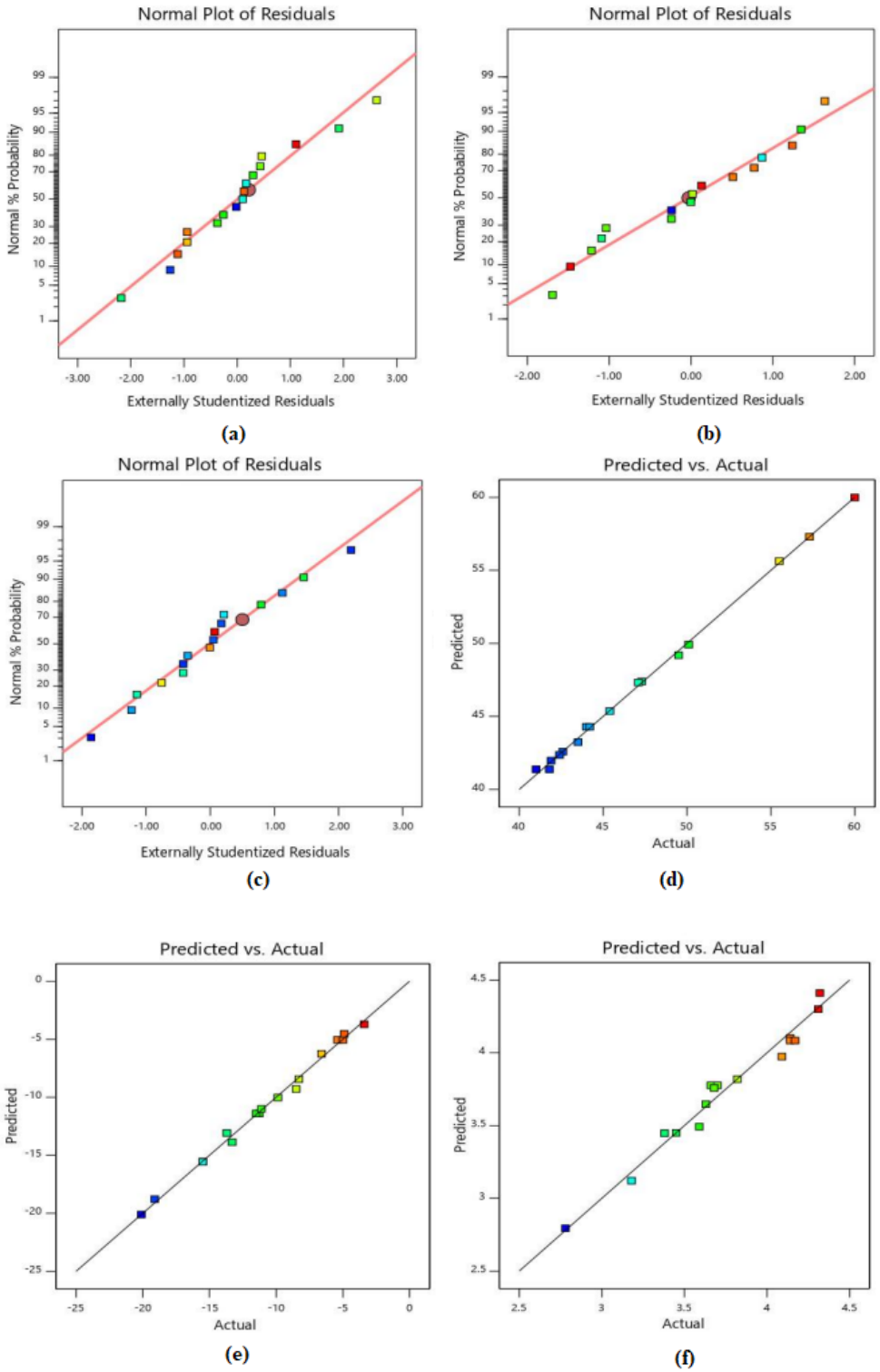

Figure 13. (**a**–**c**) Standard probability plot of the developed models; (**a**) compressive strength, (**b**) Strength reduction; (**c**) Water absorption ultimate, (**d**–**f**) Predicted vs. actual plot of the developed models; (**d**) compressive strength, (**e**) Strength reduction, (**f**) Water absorption ultimate.

Table 8. Validation properties of the response model.

Response	Compressive Strength (MPa)	Compressive Strength Reduction (%)	Water Absorption Ultimate (%)
Standard deviation	0.2777	0.4464	0.0802
Mean	47.10	−10.77	3.75
C.V %	0.5897	4.15	2.14
R^2	0.9987	0.9950	0.9723
Adjusted R^2	0.9978	0.9920	0.9654
Predicted R^2	0.9968	0.9844	0.9532
Adequate precision	101.3066	57.2138	40.2918

4. Optimization

In order to reach a mix-design with minimum compressive strength reduction and final water absorption, Design–Expert software and a multi-objective numerical optimization technique have been used. In Table 9, optimization criteria were considered to determine the optimal amounts of studied variables by explaining the project's aim, limits, and the importance of factors. The created results of multi-objective optimization for the models are shown in Figure 14 with 3D diagrams and contour lines. According to Figure 14, the optimal values of MK and SF with the highest utility (0.858) equal 34.4% and 10%, respectively. As can be seen, the elliptical nature of contour designs indicates a significant interaction between the relevant variables [56].

Table 9. Optimization benchmark.

Factors and Responses	Goals	Lower Limit	Upper Limit	Importance
MK	In range	0	40	3
SF	In range	0	10	3
Compressive strength (MPa)	In range	41	60	3
Strength reduction (%)	Maximize	−20.1	−3.4	5
Water absorption ultimate (%)	Minimize	2.78	4.32	1

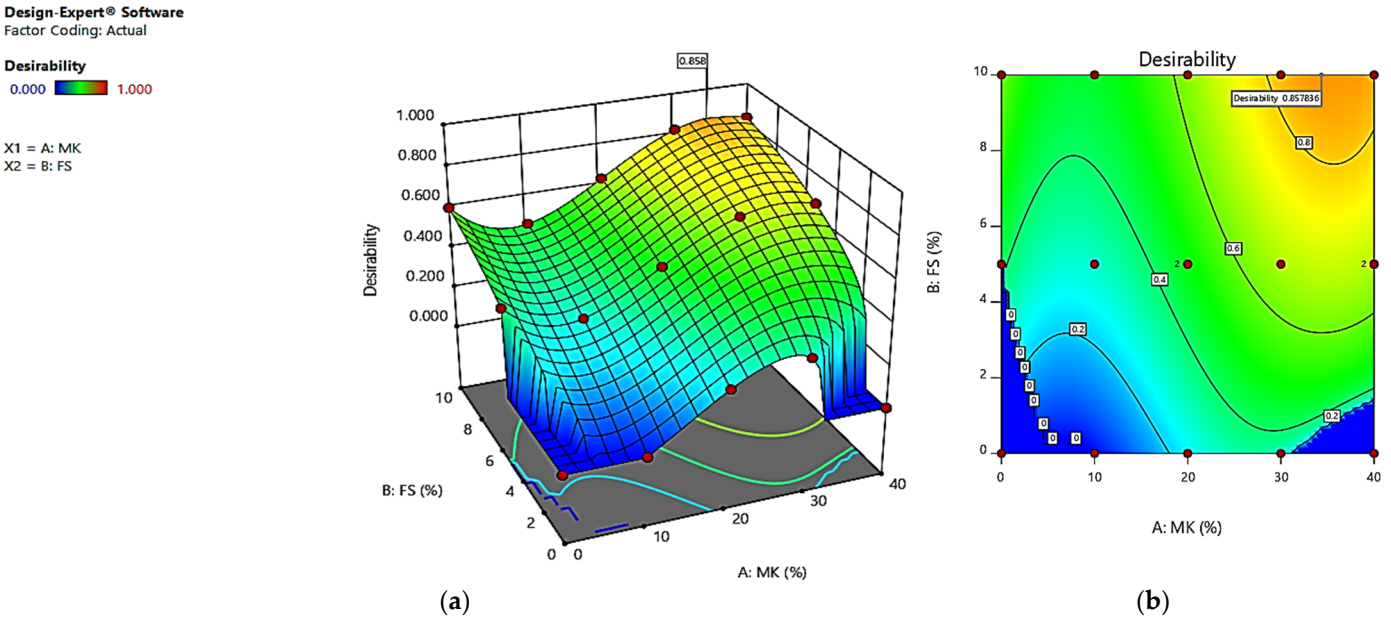

(**a**) (**b**)

Figure 14. Multi-objective optimization results for mixes containing metakaolin and silica fume (**a**) 3-D response surface model (**b**) 2-D contour plot.

5. Conclusions

This research utilized the RSM method to optimize alkali-activated slag concrete incorporating metakaolin and silica fume to enhance its resistance against sulfuric acid. Compressive strength and its reduction, water absorption, and specimen mass change have been investigated to evaluate the performance of studied alkali-activated concrete in an aggressive environment. Moreover, the microstructure of specimens was examined to this intention. Based on the experimental and analytical observation, the following results can be considered as a summary of this research's outcomes.

- In the studied specimens, the compressive strength has increased by increasing the slag content in the mix design due to the high amounts of calcium oxide. Also, 34.9 and 9% compressive strength reduction, the maximum values, have been observed in the specimens with 40, and 10% metakaolin and silica fume replacement.
- Replacing slag with metakaolin (up to 40%) increases the specimens' short-term, final, and capillary water absorption to 28.1%, 27.8%, and 10%, respectively. This is due to plate-shaped metakaolin particles with high specific surfaces which create cavities that increase water absorption.
- Maximum damage was observed in the GGBFS specimens having the most mass increase, equal to 2.31%, owing to expanding crystals forming, such as calcium sulfate (gypsum) as a reaction product of calcium oxide and sulfuric acid.
- Although increasing the slag in alkali-activated slag concrete has increased the compressive strength and decreased the permeability, the compressive strength of specimens exposed to sulfuric acid solution has reduced by 19.1% due to the solubility of $Ca(OH)_2$ in the acid solution and migration of OH^- ions. Therefore, with increasing the slag, the damage increases owing to the reaction of $Ca(OH)_2$ from calcium oxide in the slag with the sulfuric acid solution.
- The interfacing of alkali-activated concrete (AAC) with sulfuric acid (H_2SO_4) instigates a cascade of chemical reactions that can substantially deteriorate the structural integrity of the concrete. These reactions commence with neutralizing alkali activators (NaOH or KOH), dissolution of the C-S-H gel, and precipitation of gypsum ($CaSO_4 \cdot 2H_2O$) at the initial interfacing stage. As the degradation process progresses, further dissolution of the C-S-H gel, formation of ettringite ($CaAl_2(SO_4)_3 \cdot 3H_2O$), and sulfate attack ($CaSO_4 \cdot 2H_2O \rightarrow Ca(OH)_2 + 2H_2SO_4$) ensue, leading to a marked reduction in compressive strength, a surge in porosity and permeability, and the onset of cracking and spalling. These detrimental effects ultimately curtail the AAC specimens' properties, which were exposed to acidic environments.
- Based on the RSM optimization results of the studied specimens, a mix design consisting of 34.4% MK and 10% SF appears to be the most effective in achieving minimum mass change, optimal permeability, and compressive strength of alkali-activated slag-based concrete when exposed to sulfuric acid.

Author Contributions: Conceptualization, J.A.; methodology, J.A.; software, A.A., A.S. and B.B.; validation, A.S., B.B. and T.G.; formal analysis, A.A. and A.S.; investigation, A.A.; resources, A.A.; data curation, A.A.; writing—original draft preparation, A.S. and A.A.; writing—review and editing, J.A., B.B. and T.G.; visualization, J.A. and A.S.; supervision, J.A. and T.G.; project administration, J.A.; funding acquisition, J.A. and T.G. All authors have read and agreed to the published version of the manuscript.

Funding: This research received no external funding.

Data Availability Statement: The data that support the findings of this study are available from the corresponding author, upon reasonable request. The data are not publicly available due to privacy.

Conflicts of Interest: The authors have no conflicts of interest to declare that are relevant to the content of this article.

References

1. Farhan, N.A.; Sheikh, M.N.; Hadi, M.N. Investigation of engineering properties of normal and high strength fly ash based geopolymer and alkali-activated slag concrete compared to ordinary Portland cement concrete. *Constr. Build. Mater.* **2019**, *196*, 26–42. [CrossRef]
2. Aliabdo, A.A.; Abd Elmoaty, M.; Emam, M.A. Factors affecting the mechanical properties of alkali activated ground granulated blast furnace slag concrete. *Constr. Build. Mater.* **2019**, *197*, 339–355. [CrossRef]
3. Mehta, A.; Siddique, R. Sulfuric acid resistance of fly ash based geopolymer concrete. *Constr. Build. Mater.* **2017**, *146*, 136–143. [CrossRef]
4. Ariffin, M.A.M.; Bhutta, M.A.R.; Hussin, M.W.; Tahir, M.M.; Aziah, N. Sulfuric acid resistance of blended ash geopolymer concrete. *Constr. Build. Mater.* **2013**, *43*, 80–86. [CrossRef]
5. Manjunath, R.; Narasimhan, M.C. Alkali-activated concrete systems: A state of art. In *New Materials in Civil Engineering*; Butterworth-Heinemann: Oxford, UK, 2020; pp. 459–491. [CrossRef]
6. Geraldo, R.H.; Gonçalves, J.P.; Camarini, G. Mechanical properties of an eco-friendly one-part alkali-activated binder: Influence of metakaolin and water content. *Ceram. Int.* **2023**, *49*, 11854–11864. [CrossRef]
7. Jindal, B.B.; Alomayri, T.; Hasan, A.; Kaze, C.R. Geopolymer concrete with metakaolin for sustainability: A comprehensive review on raw material's properties, synthesis, performance, and potential application. *Environ. Sci. Pollut. Res.* **2022**, *30*, 25299–25324. [CrossRef] [PubMed]
8. Davidovits, J. Geopolymers: Inorganic polymeric new materials. *J. Therm. Anal. Calorim.* **1991**, *37*, 1633–1656. [CrossRef]
9. Shilar, F.A.; Ganachari, S.V.; Patil, V.B.; Reddy, I.N.; Shim, J. Preparation and validation of sustainable metakaolin based geopolymer concrete for structural application. *Constr. Build. Mater.* **2023**, *371*, 130688. [CrossRef]
10. Bakharev, T.; Sanjayan, J.G.; Cheng, Y.B. Resistance of alkali-activated slag concrete to acid attack. *Cem. Concr. Res.* **2003**, *33*, 1607–1611. [CrossRef]
11. Alzeebaree, R.; Çevik, A.; Nematollahi, B.; Sanjayan, J.; Mohammedameen, A.; Gülşan, M.E. Mechanical properties and durability of unconfined and confined geopolymer concrete with fiber reinforced polymers exposed to sulfuric acid. *Constr. Build. Mater.* **2019**, *215*, 1015–1032. [CrossRef]
12. Pacheco-Torgal, F.; Labrincha, J.; Leonelli, C.; Palomo, A.; Chindaprasit, P. (Eds.) *Handbook of Alkali-Activated Cements, Mortars and Concretes*; Elsevier: Amsterdam, The Netherlands, 2014.
13. Davidovits, J. *Geopolymer Cement. A Review*; Technical Papers; Geopolymer Institute: Saint-Quentin, France, 2013; Volume 21, pp. 1–11.
14. Bakharev, T. Resistance of geopolymer materials to acid attack. *Cem. Concr. Res.* **2005**, *35*, 658–670. [CrossRef]
15. Taylor, H.F. *Cement Chemistry*, 2nd ed.; Thomas Telford: London, UK, 1997.
16. Neville, A.M. *Properties of Concrete*; Longman: London, UK, 1995.
17. Ibrahim, M.; Johari, M.A.M.; Rahman, M.K.; Maslehuddin, M. Effect of alkaline activators and binder content on the properties of natural pozzolan-based alkali activated concrete. *Constr. Build. Mater.* **2017**, *147*, 648–660. [CrossRef]
18. Chen, W.; Brouwers, H.J.H. The hydration of slag, part 1: Reaction models for alkali-activated slag. *J. Mater. Sci.* **2007**, *42*, 428–443. [CrossRef]
19. Yip, C.K.; Lukey, G.C.; Van Deventer, J.S. The coexistence of geopolymeric gel and calcium silicate hydrate at the early stage of alkaline activation. *Cem. Concr. Res.* **2005**, *35*, 1688–1697. [CrossRef]
20. Bernal, S.A.; Rodríguez, E.D.; de Gutiérrez, R.M.; Gordillo, M.; Provis, J.L. Mechanical and thermal characterisation of geopolymers based on silicate-activated metakaolin/slag blends. *J. Mater. Sci.* **2011**, *46*, 5477–5486. [CrossRef]
21. Bernal, S.A.; Rodríguez, E.D.; de Gutiérrez, R.M.; Provis, J.L.; Delvasto, S. Activation of metakaolin/slag blends using alkaline solutions based on chemically modified silica fume and rice husk ash. *Waste Biomass Valorization* **2012**, *3*, 99–108. [CrossRef]
22. Albidah, A.; Alghannam, M.; Alghamdi, H.; Abbas, H.; Almusallam, T.; Al-Salloum, Y. Influence of GGBFS and silica fume on characteristics of alkali-activated Metakaolin-based concrete. *Eur. J. Environ. Civ. Eng.* **2023**, *27*, 3260–3283. [CrossRef]
23. Shi, C.; Shi, Z.; Hu, X.; Zhao, R.; Chong, L. A review on alkali-aggregate reactions in alkali-activated mortars/concretes made with alkali-reactive aggregates. *Mater. Struct.* **2015**, *48*, 621–628. [CrossRef]
24. Zhang, P.; Wang, K.; Li, Q.; Wang, J.; Ling, Y. Fabrication and Engineering Properties of Concretes Based on Geopolymers/Alkali-activated Binders—A Review. *J. Clean. Prod.* **2020**, *258*, 120896. [CrossRef]
25. Mobili, A.; Telesca, A.; Marroccoli, M.; Tittarelli, F. Calcium sulfoaluminate and alkali-activated fly ash cements as alternative to Portland cement: Study on chemical, physical-mechanical, and durability properties of mortars with the same strength class. *Constr. Build. Mater.* **2020**, *246*, 118436. [CrossRef]
26. Shahani, A.; Ahmadi, J.; Saeedi Razavi, B. The Effect of Using Alkaline Adhesives on the Durability of Lightweight Structural Concrete against Harmful Environments'. *Sci. Q. J. Iran. Assoc. Eng. Geol.* **2022**, *15*, 49–64.
27. Xu, H.; Van Deventer, J.S.J. The geopolymerisation of alumino-silicate minerals. *Int. J. Miner. Process.* **2000**, *59*, 247–266. [CrossRef]
28. Lee, N.K.; Lee, H.K. Setting and mechanical properties of alkali-activated fly ash/slag concrete manufactured at room temperature. *Constr. Build. Mater.* **2013**, *47*, 1201–1209. [CrossRef]
29. Bernal, S.A.; Provis, J.L.; Rose, V.; De Gutierrez, R.M. Evolution of binder structure in sodium silicate-activated slag-metakaolin blends. *Cem. Concr. Compos.* **2011**, *33*, 46–54. [CrossRef]

30. Wang, J.; Wu, X.L.; Wang, J.X.; Liu, C.Z.; Lai, Y.M.; Hong, Z.K.; Zheng, J.P. Hydrothermal synthesis and characterization of alkali-activated slag–fly ash–metakaolin cementitious materials. *Microporous Mesoporous Mater.* **2012**, *155*, 186–191. [CrossRef]
31. Ahmed, H.U.; Mohammed, A.S.; Faraj, R.H.; Abdalla, A.A.; Qaidi, S.M.; Sor, N.H.; Mohammed, A.A. Innovative modeling techniques including MEP, ANN and FQ to forecast the compressive strength of geopolymer concrete modified with nanoparticles. *Neural Comput. Appl.* **2023**, *35*, 12453–12479. [CrossRef]
32. Ahmed, H.U.; Mohammed, A.S.; Qaidi, S.M.; Faraj, R.H.; Hamah Sor, N.; Mohammed, A.A. Compressive strength of geopolymer concrete composites: A systematic comprehensive review, analysis and modeling. *Eur. J. Environ. Civ. Eng.* **2023**, *27*, 1383–1428. [CrossRef]
33. Li, C.; Sun, H.; Li, L. A review: The comparison between alkali-activated slag (Si+Ca) and metakaolin (Si+Al) cements. *Cem. Concr. Res.* **2010**, *40*, 1341–1349. [CrossRef]
34. Shi, C.; Stegemann, J.A. Acid corrosion resistance of different cementing materials. *Cem. Concr. Res.* **2000**, *30*, 803–808. [CrossRef]
35. Aiken, T.A.; Kwasny, J.; Sha, W.; Soutsos, M.N. Effect of slag content and activator dosage on the resistance of fly ash geopolymer binders to sulfuric acid attack. *Cem. Concr. Res.* **2018**, *111*, 23–40. [CrossRef]
36. Li, Z.; Lu, D.; Gao, X. Multi-objective optimization of gap-graded cement paste blended with supplementary cementitious materials using response surface methodology. *Constr. Build. Mater.* **2020**, *248*, 118552. [CrossRef]
37. Verran, G.O.; Mendes, R.P.K.; Dalla Valentina, L.V.O. DOE applied to optimization of aluminum alloy die castings. *J. Mater. Process. Technol.* **2008**, *200*, 120–125. [CrossRef]
38. Mohammed, B.S.; Haruna, S.; Liew, M.S. Optimization and characterization of cast in-situ alkali-activated pastes by response surface methodology. *Constr. Build. Mater.* **2019**, *225*, 776–787. [CrossRef]
39. Zhang, L.; Yue, Y. Influence of waste glass powder usage on the properties of alkali-activated slag mortars based on response surface methodology. *Constr. Build. Mater.* **2018**, *181*, 527–534. [CrossRef]
40. *C 127*; Standard Test Method for Density, Relative Density and Absorption of Coarse Aggregate. American Society for Testing and Materials: West Conshohocken, PA, USA, 2003.
41. *ASTM C33-03*; Standard Specification for Concrete Aggregate. Annual Book of ASTM Standards. American Society for Testing and Materials: West Conshohocken, PA, USA, 2003.
42. Rilem, T.C. 116-PCD. Permeability of concrete as a criterion of its durability. *Mater. Struct.* **1999**, *2*, 174–179.
43. *BS 1881:Part 116:1983*; Method for Determination of Compressive Strength of Concrete Cubes. British Standards Institution: London, UK, 1983.
44. *BS 1881:Part 122:1983*; Method of Determine of Water Absorption. British Standards Institution: London, UK, 1983.
45. *ASTM C 642-90*; Standard Test Method for Specific Gravity, Absorption, and Voids in Hardened Concrete. Annual Book of ASTM Standard. American Society for Testing and Materials: West Conshohocken, PA, USA, 1990.
46. Xiang, J.; He, Y.; Liu, L.; Zheng, H.; Cui, X. Exothermic behavior and drying shrinkage of alkali-activated slag concrete by low temperature-preparation method. *Constr. Build. Mater.* **2020**, *262*, 120056. [CrossRef]
47. Zamanabadi, S.N.; Zareei, S.A.; Shoaei, P.; Ameri, F. Ambient-cured alkali-activated slag paste incorporating micro-silica as repair material: Effects of alkali activator solution on physical and mechanical properties. *Constr. Build. Mater.* **2019**, *229*, 116911. [CrossRef]
48. Davidovits, J. *Why Alkali-Activated Materials (AAM) Are Not Geopolymers*; Publication Technical Paper; Geopolymer Institute Library: Saint-Quentin, France, 2018; Volume 25.
49. Liu, J.; Doh, J.H.; Ong, D.E.; Liu, Z.; Hadi, M.N. Methods to evaluate and quantify the geopolymerization reactivity of waste-derived aluminosilicate precursor in alkali-activated material: A state-of-the-art review. *Constr. Build. Mater.* **2023**, *362*, 129784. [CrossRef]
50. Marvila, M.T.; Azevedo, A.R.; Vieira, C.M. Reaction mechanisms of alkali-activated materials. *Rev. IBRACON Estrut. Mater.* **2021**, *14*, e14309. [CrossRef]
51. Hojati, M.; Radlińska, A. Shrinkage and strength development of alkali-activated fly ash-slag binary cements. *Constr. Build. Mater.* **2017**, *150*, 808–816. [CrossRef]
52. Lee, N.K.; Jang, J.G.; Lee, H.K. Shrinkage characteristics of alkali-activated fly ash/slag paste and mortar at early ages. *Cem. Concr. Compos.* **2014**, *53*, 239–248. [CrossRef]
53. Najimi, M.; Ghafoori, N. Engineering properties of natural pozzolan/slag based alkali-activated concrete. *Constr. Build. Mater.* **2019**, *208*, 46–62. [CrossRef]
54. Wang, A.; Zheng, Y.; Zhang, Z.; Liu, K.; Li, Y.; Shi, L.; Sun, D. The durability of alkali-activated materials in comparison with ordinary Portland cements and concretes: A review. *Engineering* **2020**, *6*, 695–706. [CrossRef]
55. Mohammed, B.S.; Achara, B.E.; Nuruddin, M.F.; Yaw, M.; Zulkefli, M.Z. Properties of nano-silica-modified self-compacting engineered cementitious composites. *J. Clean. Prod.* **2017**, *162*, 1225–1238. [CrossRef]
56. Aydın, S. A ternary optimization of mineral additives of alkali activated cement mortars. *Constr. Build. Mater.* **2013**, *43*, 131–138. [CrossRef]